# Cross section measurements for neutron inelastic scattering and the $(n, 2n\gamma)$ reaction on $^{206}$Pb

A. Negret,[1,*] L. C. Mihailescu,[1,2,†] C. Borcea,[1] Ph. Dessagne,[3,4] K. H. Guber,[5] M. Kerveno,[3,4] A. J. Koning,[6] A. Olacel,[1,7] A. J. M. Plompen,[2] C. Rouki,[2] and G. Rudolf[3,4]

[1]*"Horia Hulubei" National Institute for Physics and Nuclear Engineering, R-077125 Bucharest-Măgurele, Romania*
[2]*European Commission, Joint Research Centre, Institute for Reference Materials and Measurements, B-2440 Geel, Belgium*
[3]*Université de Strasbourg, IPHC, F-67037 Strasbourg, France*
[4]*CNRS, UMR7178, F-67037 Strasbourg, France*
[5]*Reactor and Nuclear Systems Division, Oak Ridge National Laboratory, Oak Ridge, Tennessee 37831, USA*
[6]*Nuclear Research Group Petten, NL-1755 ZG Petten, The Netherlands*
[7]*University of Bucharest, Faculty of Physics, R-077125, Bucharest-Măgurele, Romania*

(Received 27 May 2015; published 30 June 2015)

Excitation functions for $\gamma$ production associated with the neutron inelastic scattering and the $(n, 2n)$ reactions on $^{206}$Pb were measured from threshold up to 18 MeV for about 40 transitions. Two independent measurements were performed using different samples and acquisition systems to check consistency of the results. The neutron flux was determined with a $^{235}$U fission chamber and a procedure that were validated against a fluence standard. For incident energy higher than the threshold for the first excited level and up to 3.5 MeV, estimates are provided for the total inelastic and level cross sections by combining the present $\gamma$ production cross sections with the level and decay data of $^{206}$Pb reported in the literature. The uncertainty common to all incident energies is 3.0% allowing overall uncertainties from 3.3% to 30% depending on transition and neutron energy. The present data agree well with earlier work, but significantly expand the experimental database while comparisons with model calculations using the TALYS reaction code show good agreement over the full energy range.

DOI: 10.1103/PhysRevC.91.064618 PACS number(s): 25.40.Fq, 29.30.Kv, 27.80.+w, 24.10.−i

## I. INTRODUCTION

Nuclear data with low uncertainties are needed for the design of future generation nuclear facilities [generation-IV reactors and accelerator driven systems (ADS)]. Lead is considered as the coolant for such reactors. Sensitivity studies for ADS [1] showed that the required uncertainty for inelastic scattering cross sections of lead isotopes below 20 MeV is about 10%, while for the $(n, 2n)$ reaction it is of the order of 20%. For lead-cooled fast reactors a similar sensitivity study resulted in a required uncertainty of about 5% for inelastic scattering cross sections of $^{206}$Pb for an incident neutron energy below 6 MeV [2]. Those sensitivity studies propagate nuclear data uncertainties to determine the precision of estimates of key reactor parameters (effective multiplication factor, power peak, coolant void and temperature reactivity coefficients, and change of reactivity from beginning to end of the fuel cycle). Required nuclear data uncertainties follow from the constraints imposed by the target uncertainties on such estimates. The firm requirements from the lead-cooled fast reactor are largely from the use of more stringent uncertainties imposed on these reactor parameters. With similar tight requirements for an ADS the required uncertainty for the $^{206}$Pb inelastic scattering cross section becomes 3%–4% [3]. The accuracy of the inelastic scattering cross section is essential because the process represents the dominant mechanism for energy loss in the systems where light elements and particularly hydrogen are absent.

Neutron inelastic and $(n, 2n)$ data for $^{206}$Pb of the required accuracy and completeness are a challenge both experimentally and theoretically. Experimentally the required accuracy is within reach but only for part of the required data. Theoretical models can provide the full range of cross sections, emitted particle spectra, and angular distributions but lack the accuracy. While the main motivation for the present investigation comes from the strict demands set by applications, it is absolutely necessary to use a judicious combination of extremely precise experimental techniques and state-of-the-art model calculations to achieve the goal.

Neutron inelastic scattering cross sections for $^{206}$Pb were previously measured using either the $(n, n')$ technique, i.e., by detection of the outgoing neutrons, or the $(n, n'\gamma)$ technique detecting the associated $\gamma$ rays. Measurements with the first technique [4–9] were performed at energies between 2 and 8 MeV. These experiments measured the differential cross sections for the first excited levels or determined level density parameters from the emission spectra [7,10]. The $(n, n'\gamma)$ technique was used in Refs. [11–17] either with Ge(Li) or with NaI detectors. Most of these works used radiogenic samples with about 88% $^{206}$Pb. Concerning the $^{206}$Pb$(n,2n)$ reaction, Jönsson *et al.* [13] determined a $\gamma$ production cross section for the 987.7-keV transition of $^{205}$Pb, Salaita and Eapen [18] and Garg and Khurana [19] determined isomeric cross sections by the activation technique while Fréhaut *et al.* [20] determined the total $(n,2n)$ cross section by counting the emitted neutrons. Important complementary data for modeling and a discussion of the nonelastic cross section of $^{206}$Pb are those for the total cross section [4,21–28] and the elastic scattering angular distribution and cross section [29–35].

*alnegret@tandem.nipne.ro
†Present address: Studiecentrum voor Kernenergie - Centre d'Etude de l'Energie Nucleaire, B-2400 Mol, Belgium.

 

Here we primarily aim at providing a new large data set for inelastic scattering with the best achievable accuracy for the cross section and the highest achievable resolution for the incident energy.

A new experiment was performed at the Geel Linear Accelerator (GELINA) neutron time-of-flight facility to significantly improve the knowledge on the neutron inelastic and $(n, 2n\gamma)$ cross sections for $^{206}$Pb below 20 MeV. The $(n, xn\gamma)$ technique was used. The $\gamma$ rays from the $^{206}$Pb$(n, xn\gamma)$ reaction ($x = 1$ and 2) were detected with four large volume HPGe (high-purity germanium) detectors. The high energy resolution of the germanium detectors allowed clear identification of the $\gamma$ rays. A precise angle integration was possible placing the detectors at 110° and 150° with respect to the neutron beam direction. The full energy range from threshold up to about 20 MeV was covered with a neutron energy resolution of 1.3 keV at 1 MeV (42 keV at 10 MeV) for the strongest $\gamma$ rays. The measured cross sections were normalized to the standard $^{235}$U($n$,$f$) cross section [36] using a new procedure that was validated by an intercomparison with reference fluence measurement instruments of Physikalisch-Technische Bundesanstalt (PTB). Two independent measurements were performed using different acquisition systems and different samples. The results of the two measurements agree very well increasing the confidence in the results.

At least one $\gamma$ ray was observed from the decay of the levels up to 2236.5 keV with the exception of the $J^\pi = 0^+$ level at 1166.4 keV and the 180-$\mu$s isomer at 2200.2-keV excitation energy. Above 2236.5 keV, for more and more levels a decaying $\gamma$ ray was not observed, the maximum excitation energy of a level with an observed decay being 3606.2 keV. The $\gamma$ production cross section was measured for 34 $\gamma$ rays from the inelastic channel. Two $\gamma$ rays from the $^{206}$Pb$(n, 2n\gamma)^{205}$Pb reaction were also observed: 703.4 keV and 987.6 keV. No $\gamma$ rays from the first two excited levels of the $^{205}$Pb nucleus were observed because of their low energy.

For the $^{206}$Pb nucleus there are two major limitations in the use of the $(n, n'\gamma)$ technique in addition to the inherent limitation that no information is obtained about the scattered neutron's angular distribution. The first one is the presence of an E0 transition that dominates the decay of the second excited level at 1166.4 keV ($J^\pi = 0^+$) to the ground state [37]. This transition is fully converted internally and therefore it cannot be observed with HPGe detectors. The $\gamma$ decay of the $0^+$ level to the first excited level is so weak that it could not be observed by us nor in earlier work. The second limitation concerns an isomer at 2200.2 keV with a lifetime of 180(3) $\mu$s [37]. The $\gamma$ rays from the decay of this isomer (516.2 and 202.4 keV) are delayed and almost all of the decay occurs outside of the 24-$\mu$s time span of the present measurement. Therefore the $\gamma$ rays emitted following the decay of the isomer are hard to observe and in practice, no measurable yield was found below the inelastic threshold for a transition associated with its decay (e.g., the 881.0-keV $\gamma$ ray that occurs after the 516.2-keV transition of the isomer). With these limitations in mind we constructed total and level inelastic cross sections based on the $\gamma$ production data and the adopted level and decay scheme [37].

To investigate the status of modeling we compare this new data set with state of the art calculations using both a fully phenomenological approach and a microscopic approach. The phenomenological approach uses parameters optimized globally [38–41]. The microscopic approach uses optical model parameters, strength functions and level densities calculated on the basis of effective nuclear interactions and combinatorics [41–45]. In both cases Version 1.6 of the TALYS reaction code was used [46,47].

## II. EXPERIMENTAL SETUP AND DATA ANALYSIS

Detailed descriptions of the experimental setup and data analysis were given in Refs. [48–50]. Here, we focus on describing the specific points of the present experiment and refer to those references for further details.

### A. Experimental setup

The measurements were performed at the GELINA neutron time-of-flight facility of the European Commission, Joint Research Center, Institute for Reference Materials and Measurements (EC-JRC-IRMM). An electron linear accelerator produces 1-ns pulses with a mean energy of 100 MeV at a repetition rate of 800 Hz. The average current is $\approx$7 $\mu$A. The electrons impinge on a rotary depleted uranium target producing bremsstrahlung. The neutron spectrum with energies between 800 keV and 18 MeV from $(\gamma,xn)$ and $(\gamma,F)$ reactions is used. A detailed description of the facility can be found in Refs. [51–53].

Two measurements were carried out by detecting $\gamma$ rays emitted in the $(n,xn\gamma)$ reactions using HPGe detectors. In the first measurement (further labeled "Exp I") a large radiogenic lead sample and a fast digitizer-based data acquisition system were used. The second one ("Exp II") used a highly enriched, smaller $^{206}$Pb sample and classical electronics and data acquisition. Table I gives the details of the samples. The radiogenic Pb was characterized by isotope mass spectrometry at IRMM, while the amount fractions for the enriched sample

TABLE I. Sample characteristics for the two measurements. Sample mass, diameter ($d$), thickness ($t$), and isotope amount fractions are given (atom %). Uncertainties represent one standard deviation, throughout this work.

| Measurement | Mass (g) | $d$ (mm) | $t$ (mm) | $^{204}$Pb (%) | $^{206}$Pb (%) | $^{207}$Pb (%) | $^{208}$Pb (%) |
|---|---|---|---|---|---|---|---|
| Exp I (radiogenic sample) | 215.48(1) | 69.8(1) | 5.01(1) | 0.0749(3) | 88.59(3) | 8.46(4) | 2.87(2) |
| Exp II (enriched sample) | 43.2781(7) | 50.0(2) | 2.02(4) | $< 0.01$ | 99.82(3) | 0.16(2) | 0.02(1) |

TABLE II. Low excitation levels and $\gamma$ transitions in $^{206}$Pb. All energy, spin, and parity and branching ratio values are from the evaluated level scheme [37]. The levels and $\gamma$'s for which we determined the production cross sections are emphasized with bold characters.

| $E_L$ (keV) | $J^\pi$ | $E_\gamma$ (keV) | Branching ratio (%) | Final level | | Notes |
|---|---|---|---|---|---|---|
| **803.1** | $2^+$ | **803.1**[a] | 100 | 0 | $0^+$ | |
| 1166.4 | $0^+$ | 363.3 | $\leqslant$0.24 | 803.1 | $2^+$ | Very weak, not observed |
| | | 1166.4 | | 0 | $0^+$ | E0, completely converted |
| **1340.5** | $3^+$ | **537.5** | 100 | 803.1 | $2^+$ | |
| **1466.8** | $2^+$ | 126.4 | 3.8(4) | 1340.5 | $3^+$ | |
| | | 663.8 | 100(1) | 803.1 | $2^+$ | |
| | | **1466.8**[a] | 30.4(7) | 0 | $0^+$ | |
| **1684.0** | $4^+$ | **343.5** | 35.4(5) | 1340.5 | $3^+$ | |
| | | **881.0** | 100(1) | 803.1 | $2^+$ | |
| **1704.5** | $1^+$ | **1704.5**[a] | 100 | 0 | $0^+$ | |
| **1784.1** | $2^+$ | 317.5 | 23(3) | 1466.8 | $2^+$ | |
| | | 617.6 | 11(3) | 1166.4 | $0^+$ | |
| | | **981.0**[a] | 100(4) | 803.1 | $2^+$ | |
| | | 1784.7 | 5.2(15) | 0 | $0^+$ | |
| **1997.7** | $4^+$ | 313.7 | 21(2) | 1684.0 | $4^+$ | |
| | | **657.2** | 100(2) | 1340.5 | $3^+$ | |
| | | 1194.7 | 14.5(8) | 803.1 | $2^+$ | |
| **2149.0** | $2^+$ | 682.3 | 20(3) | 1466.8 | $2^+$ | |
| | | 808.6 | 20(3) | 1340.5 | $3^+$ | |
| | | **1345.9** | 100(5) | 803.1 | $2^+$ | |
| **2196.7** | $(3)^+$ | 729.2 | 7(3) | 1466.8 | $2^+$ | |
| | | **856.6** | 100 | 1340.5 | $3^+$ | |
| | | **1393.8** | 78(5) | 803.1 | $2^+$ | |
| 2200.2 | $7^-$ | 202.4 | 0.11(1) | 1997.7 | $4^+$ | Isomer, $T_{1/2}$=125 $\mu$s |
| | | 516.2 | 100(1) | 1684.0 | $4^+$ | Not observed |
| 2236.5 | | **1433.5**[b] | 100 | 803.1 | $2^+$ | |
| 2314 | $0^+$ | | | | | |
| 2384.2 | $6^-$ | 184.0 | 100 | 2200.2 | $7^-$ | |
| 2391.3 | | **1588.2** | 100 | 803.1 | $2^+$ | $\gamma$ not separated from the 1588.6-keV $\gamma$ ray |
| **2423.4** | $2^+$ | 639.0 | 4.9(13) | 1784.1 | $2^+$ | |
| | | **718.9** | 48.5(20) | 1704.5 | $1^+$ | |
| | | **956.6**[b] | 20.6(16) | 1466.8 | $2^+$ | |
| | | 1082.7 | 8.5(16) | 1340.5 | $3^+$ | |
| | | **1620.3** | 100(4) | 803.1 | $2^+$ | |
| **2647.8** | $3^-$ | 964.2 | 6.4(7) | 1684.0 | $4^+$ | |
| | | **1844.5** | 100(4) | 803.1 | $2^+$ | |
| 2658.3 | $9^-$ | 458.1 | 100 | 2200.2 | $7^-$ | |
| 2782.2 | $5^-$ | **398.0** | 79.6(7) | 2384.2 | $6^-$ | |
| | | 582.0 | 3.59(18) | 2200.2 | $7^-$ | |
| | | 784.6 | 3.97(7) | 1997.7 | $4^+$ | |
| | | **1098.3** | 100(11) | 1684.0 | $4^+$ | |
| 2826.3 | $(4)^+$ | 44.1 | 6.4(8) | 2782.2 | $5^-$ | |
| | | 434.9 | 20.5(18) | 2391.3 | | |
| | | 442.1 | 34(4) | 2384.2 | $6^-$ | |
| | | **1142.4**[b] | 100(4) | 1684.0 | $4^+$ | |
| | | 2022.8 | 11.6(18) | 803.1 | $2^+$ | |
| 2864.6 | $7^-$ | 480.4 | 91(9) | 2384.2 | $6^-$ | |
| | | 664.2 | 100(5) | 2200.2 | $7^-$ | |
| | | **1180.7**[b] | 68(7) | 1684.0 | $4^+$ | |
| 2929.1 | $4^+$ | **1588.6** | 100 | 1340.5 | $3^+$ | $\gamma$ not separated from the 1588.2-keV $\gamma$ ray |
| 2939.6 | $6^-$ | 157.5 | 22.6(25) | 2782.2 | $5^-$ | |
| | | 555.3 | 23.9(25) | 2384.2 | $6^-$ | |
| | | **739.2** | 100(5) | 2200.2 | $7^-$ | |

TABLE II. (*Continued.*)

| $E_L$ (keV) | $J^\pi$ | $E_\gamma$ (keV) | Branching ratio (%) | Final level | | Notes |
|---|---|---|---|---|---|---|
| 2954.5 | $8^-$ | 296.2 | 68(8) | 2658.3 | $9^-$ | |
| | | 754.4 | 100(8) | 2200.2 | $7^-$ | |
| 2960 | | | | | | |
| 2984 | $2^+$ | | | | | |
| 3016.4 | $5^-$ | 190.0 | 22.6(25) | 2826.3 | $(4)^-$ | |
| | | 234.2 | 5.4(3) | 2782.2 | $5^-$ | |
| | | **632.3** | 100(1) | 2384.2 | $6^-$ | |
| | | 816.3 | | 2200.2 | $7^-$ | |
| | | 1332.3 | 6.3(3) | 1684.0 | $4^+$ | |
| 3033 | | | | | | |
| 3122.4 | $(3^+)$ | 1655.5 | 28(7) | 1466.8 | $2^+$ | |
| | | **2319.3**[b] | 100(10) | 803.1 | $2^+$ | |
| 3139 | | | | | | |
| 3194 | $(5^-)$ | | | | | |
| 3194.3 | (1,2) | 2391.0 | 65(15) | 803.1 | $2^+$ | |
| | | **3194.6** | 100(19) | 0 | $0^+$ | |
| 3225.4 | $(5,6,7)^-$ | 360.8 | | 2864.6 | $7^-$ | |
| | | 443.2 | | 2782.2 | $5^-$ | |
| | | 841.3 | 100(5) | 2384.2 | $6^-$ | |
| | | 1025.3 | 22.9(21) | 2200.2 | $7^-$ | |
| 3244.2 | $4^-$ | 227.7 | | 3016.4 | $5^-$ | |
| | | 1047.6 | 18(9) | 2196.7 | $(3)^+$ | |
| | | 1246.5 | 22.2(21) | 1997.7 | $4^+$ | |
| | | **1560.3** | 100(5) | 1684.0 | $4^+$ | |
| | | **1903.6** | 92(4) | 1340.5 | $3^+$ | |
| | | 2439.0 | 1.3(5) | 803.1 | $2^+$ | |
| 3260.4 | $6^+$ | 1576.4 | 100 | 1684.0 | $4^+$ | |
| 3279.2 | $5^-$ | 35.0 | 0.11(1) | 3244.2 | $4^-$ | |
| | | 262.7 | 19.3(3) | 3016.4 | $5^-$ | |
| | | 339.9 | | 2939.6 | $6^-$ | |
| | | 452.8 | 1.00(5) | 2826.3 | $(4)^-$ | |
| | | **497.1**[b] | 97.8(10) | 2782.2 | $5^-$ | |
| | | 895.1 | 100(1) | 2384.2 | $6^-$ | |
| | | 1281.8 | 0.42(4) | 1997.7 | $4^+$ | |
| | | 1595.3 | 32.0(4) | 1684.0 | $4^+$ | |
| | | 2476.7 | 0.09(1) | 803.1 | $2^+$ | |
| 3328 | | | | | | |
| 3377 | | | | | | |
| 3402.7 | $5^-$ | 620.5 | 18.1(2) | 2782.2 | $5^-$ | Weak, not observed transitions to 3279.2-, 3244.2-, 3016.4-, 2939.6-, 2826.3-, 2647.8-, 2200.2-, and 803.1-keV levels |
| | | 1018.6 | 23.8(3) | 2384.2 | $6^-$ | |
| | | 1405.0 | 4.50(8) | 1997.7 | $4^+$ | |
| | | **1718.7** | 100 | 1684.0 | $4^+$ | |
| 3453 | $5^-$ | | | | | |
| 3453.4 | $4^+$ | **2650.3**[b] | 100 | 803.1 | $2^+$ | |
| 3484.8 | | 1699.5 | 54(14) | 1784.1 | $2^+$ | |
| | | **2682.0**[b] | 100(18) | 803.1 | $2^+$ | |
| 3516 | $(4^+)$ | 2713 | 100 | 803.1 | $2^+$ | |
| 3562.9 | $5^-$ | 1565.3 | 15.1(7) | 1997.7 | $4^+$ | Weak, not observed transitions to 3279.2-, 2782.2-, 2647.8-, and 803.1-keV levels. |
| | | **1878.7** | 100(2) | 1684.0 | $4^+$ | |
| 3606.2 | $2^+$ | 957.9 | 64(13) | 2647.8 | $3^-$ | |
| | | **1822.1**[b] | 100 | 1784.1 | $2^+$ | |
| 3623 | $4^+$ | | | | | |

[a] $\gamma$ rays that were used for the construction of the total inelastic cross section.
[b] $\gamma$ rays observed only in the first measurement from better statistics.

were provided by the Oak Ridge National Laboratory's Isotope Office, from which both samples were borrowed. Each measurement used four detectors but two of those used in the first measurement were replaced by two others in the second one. The relative efficiencies of the detectors ranged from 95% to 100% in Exp I and from 76% to 105% in Exp II. The two measurements allow for a careful check of the methods of data taking and data analysis and have served to commission a new digitizer-based data acquisition system.

The sample was positioned at a distance of 198.551 m from the neutron source and the beam was collimated to a diameter of 61 mm. The distance between the sample and the front of the detectors ranged between 13.6 and 14.7 cm. In both measurements two detectors were placed at 110° and two at 150° so that a weighted sum of the differential cross sections at these two angles provided an accurate angle-integrated cross section for transitions with multipolarity up to 3 by the principle of the Gauss quadrature [48].

Data acquisition in Exp I involved two DC440 Aquiris digitizer cards (420 million samples per second, 12 bits sampling resolution) with two inputs each. These were controlled by a PC that processed the waveforms to obtain the time and amplitude of the registered events and stored these in list files. A separate trigger generated when a neutron-induced event occurs is provided to each card. The trigger time is determined by the arrival time of the electron burst at the neutron producing target. The acquired waveforms ranged from a microsecond before arrival of the $\gamma$ flash from the bremsstrahlung from the neutron target to a few microseconds after the time of flight for the lowest neutron energy of interest (i.e., the time of flight of ≈800-keV neutrons). A detailed description of the processing algorithms, tests, and performances of the acquisition system was presented in Ref. [50]. Data acquisition in Exp II is based on classical electronics as described in Refs. [48,49].

The neutron flux was permanently monitored using a multilayer fission chamber with 3.066(6) mg/cm$^2$ of $^{235}$U evenly distributed over eight deposits. The active diameter (70 mm) of the fission chamber was larger than the beam diameter. The fission chamber was placed at a distance of 197.214 m from the neutron source, in front of the sample.

### B. Data analysis

Raw data were sorted into time of flight versus pulse height matrices. Time-of-flight bins of 9.5 ns for Exp I and 8 ns for Exp II were used resulting in a resolution of 1.3 keV at 1 MeV and 42 keV at 10 MeV for Exp I (1.1 and 35 keV, respectively, for Exp II). For lower yields (depending on transition and neutron energy) the bin sizes were increased to obtain a reasonable number of counts per bin.

The photopeak efficiency of the HPGe detectors was measured using pointlike sources placed in the sample position. The measured efficiencies were corrected for the extended volume and for the self-attenuation of the $\gamma$ rays in the sample. These corrections were performed by means of simulations using the MCNP [54] code. The total uncertainty on the HPGe efficiency was between 1.7% and 2.1% up to 1.4-MeV $\gamma$-ray energy and about 4.5% for the $\gamma$ rays with energy higher than 1.4 MeV. The uncertainty of the activity of the $^{152}$Eu calibration source was 0.7%. The main contribution to the uncertainty is from the Monte Carlo model of the setup [55].

The $\gamma$ production cross sections for the $^{206}$Pb$(n, n'\gamma)^{206}$Pb reaction were also corrected for the attenuation and multiple scattering of the neutrons in the sample using MCNP simulations. For the most intense $\gamma$ ray (803.1 keV), this correction is smaller than 1.5% below $E_n = 8.1$ MeV and it increases fast above this energy because of the opening of the $(n, 2n)$ channel. At 18 MeV it reaches about 50%. For the other transitions the reaction threshold increases and above 8.1 MeV the correction for the neutron attenuation and multiple scattering is smaller (less than 10% for all $\gamma$ rays). The statistical uncertainties of the MCNP simulations were negligible.

Because of the high $^{207}$Pb content of the radiogenic sample (8.5%), corrections were required in Exp I for the $^{207}$Pb$(n, 2n\gamma)$ contributions to the $^{206}$Pb$(n,n\gamma)$ reaction. These were performed for the two strongest inelastic transitions (803.1 and 537.5 keV) using the $^{207}$Pb$(n, 2n\gamma)$ cross sections reported in Ref. [56].

The $^{235}$U$(n, f)$ cross section of Ref. [36] was used to normalize the cross sections presented here. It should be noted that our current method for determining the fission chamber efficiency differs significantly from that published in Ref. [48] and the resulting estimate is notably different. The new value for the efficiency of detecting a fission event is 0.861(10). This is about 12% lower than the value in Ref. [48] and results in higher cross sections than reported in Ref. [56]. The new method for determining this efficiency was validated by comparison with a recoil proton telescope, a $^{235}$U fission chamber, a $^{238}$U fission chamber, and a NE213 liquid scintillator at the PTB [57–59].

The total inelastic and the level cross sections were constructed using the angle integrated $\gamma$ production cross sections and the evaluated level scheme of $^{206}$Pb [37] as it is described in Refs. [48,49].

For several excited levels in $^{206}$Pb the $\gamma$ production cross section was measured for more than one $\gamma$ ray. In these cases the branching ratios were also determined.

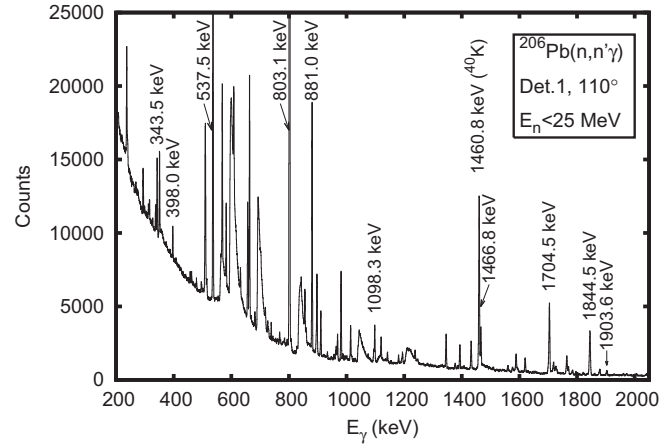


FIG. 1. $\gamma$-ray spectrum recorded with a HPGe detector and with the $^{\text{radiogenic}}$Pb sample. The spectrum was integrated over neutron energies lower than ≈25 MeV. The main $\gamma$-ray peaks from the inelastic scattering on $^{206}$Pb are clearly visible.

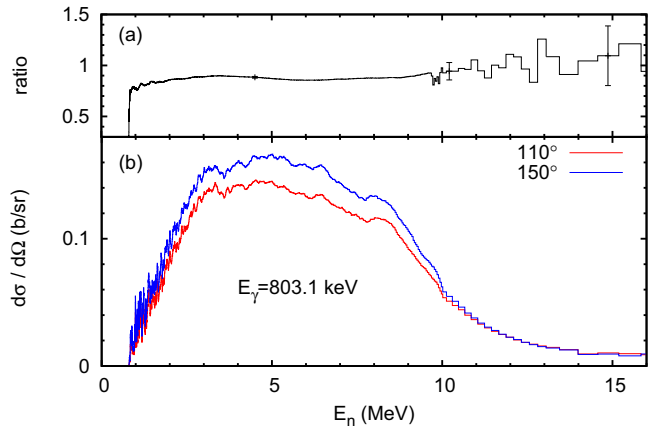


FIG. 2. (Color online) Differential $\gamma$ production cross section for the 803.1-keV transition in $^{206}$Pb at 110° and 150° together with the ratio between the differential cross section values. The present data were smoothed with an averaging moving window filter for an easier comparison.

## III. REACTION CALCULATIONS WITH TALYS 1.6

TALYS [60] is a well-known software used both for the analysis of reaction experiments and for generating nuclear data [47]. The main advantage of the code resides in its completeness: It implements in a unified approach various reaction mechanisms (direct, compound, multistep, and fission processes) integrating ECIS-06 code [61] as a routine used for optical model and coupled-channels calculations. The default optical model parameters used by TALYS are those from Ref. [38]. The multistep processes (preequilibrium) are described in the exciton model [39]. TALYS can be used over a very wide energy range (from 1 keV to 200 MeV) for target nuclei with the mass number $A = 12$–$339$.

An interesting feature of the code is the possibility of performing a reasonable calculation using only default parameters. Based on a global analysis of the available data [38–40,42–46] TALYS provides default values for practically all input parameters required and, based on this feature, the code claims very strong predictive power.

The structure of $^{206}$Pb at low excitation energies is described by two neutron holes in the double-magic nucleus $^{208}$Pb. To describe the $^{206}$Pb$(n, xn\gamma)$ reactions TALYS employs the optical model together with DWBA and the multistep theory. The threshold for the inelastic reaction is $E_{\rm th}^{\rm inel} = 807.0$ keV. Immediately after the threshold the inelastic cross section is dominated by the compound nucleus mechanism. As the energy of the incoming neutron increases, the direct and preequilibrium mechanisms play a more important role while various inelastic channels open. The threshold of the $^{206}$Pb$(n, 2n)^{205}$Pb reaction is $E_{\rm th}^{(n,2n)} = 8126.3$ keV.

For a proper comparison with the experimental data, two corrections are necessary for the production cross section of the 803.1-keV $\gamma$ ray (as well as for other transitions) given by the TALYS calculation. The first one regards the presence of an isomeric level at 2200.2 keV. The TALYS code neglects the long lifetime of this level and the $\gamma$ rays from the isomer are considered as prompt transitions. For the comparison with the present measurement, the cross sections of the $\gamma$ rays that decay from the isomer (516.2 and 202.4 keV) have to be subtracted from the cross sections of all $\gamma$ rays that I fed through the isomer.

The second correction regards the presence of the E0 transition. The TALYS code attributes the full decay strength of the 1166.4-keV, $0^+$ level to the 363.3-keV transition that feeds the first excited level. This is contrary to the information in the latest evaluated level scheme [37], where the 363.3-keV transition has negligible intensity (less than 0.24%). Therefore the calculated $\gamma$ production cross section of the 363.3-keV transition has to be subtracted from the calculated $\gamma$ production cross section of the 803.1-keV transition to make a correct comparison. In practice, both corrections were performed by altering the structure files used by TALYS.

## IV. RESULTS AND DISCUSSION

The experimental results obtained with both measured samples are presented below. The $\gamma$ production cross sections are shown in Sec. IV A for all observed transitions together with examples of differential $\gamma$ production cross sections at 110° and 150°. For several excited levels in $^{206}$Pb, at least two $\gamma$

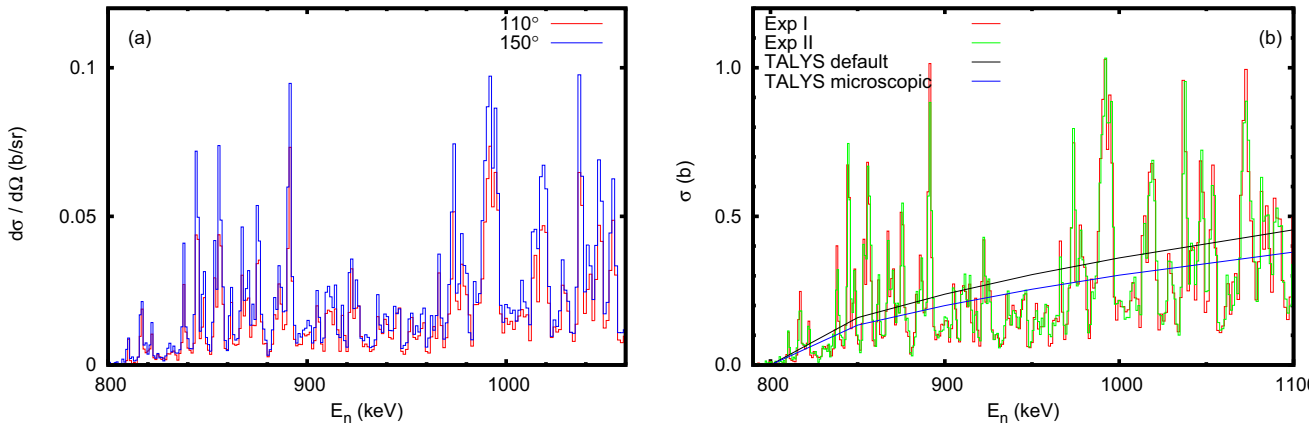


FIG. 3. (Color online) Full resolution $\gamma$ production cross section for the 803.1-keV transition in $^{206}$Pb. (a) Differential $\gamma$ production cross section at 110° and 150°. (b) Integral $\gamma$ production cross section compared with TALYS calculation.

rays were observed and the branching ratios were determined. The total inelastic and the level cross sections are given in Sec. IV B.

### A. $\gamma$ production cross sections

Table II lists all known levels and transitions from $^{206}$Pb according to the evaluated level scheme [37]. The levels and $\gamma$'s for which we determined the production cross sections are emphasized with bold characters. Some $\gamma$ transitions were observed only in the first measurement where the statistics was slightly better. Figure 1 shows an example of the amplitude spectrum obtained with one of the HPGe detectors and the $^{\text{radiogenic}}$Pb sample. The main peaks from the $^{206}$Pb$(n,n'\gamma)^{206}$Pb reaction are marked.

#### *1. The 803.1-keV transition*

In $^{206}$Pb the transition from the first excited level to the ground state is by far the most intense in the spectrum. The 803.1-keV $\gamma$ ray is an E2 transition from the initial $2^+$ level to the $0^+$ ground state. A clear angle dependence of the differential $\gamma$ production cross section was observed (Fig. 2). The ratio between the differential cross section at 110° and 150° has a minimum just above the inelastic threshold and it increases at higher energies becoming almost 1 for $E_n \geqslant 10$ MeV. This trend is confirmed by a calculation with the CINDY code [62].

As in the cases of the $^{52}$Cr [49] and $^{56}$Fe [63] nuclei studied with the same experimental setup, well-defined resonance structures were observed for $^{206}$Pb. The resonance structures in the differential and the integral $\gamma$ production cross sections are shown in Fig. 3. The observation of these resonances was possible because of the very good neutron energy resolution. The results from two measurements agree very well [Fig. 3(b)].

In our previous studies [63,64] we attempted an understanding of the structures observed in our cross sections by comparing the number of resonances directly counted with the theoretical level density estimated using the back-shifted Fermi gas model formula parametrized in Ref. [65]. We concluded that for the first 500 keV after the opening of the inelastic channel the structures may correspond to individual levels in the compound nucleus. However, above this range, the theoretical level density diverges severely from the number of resonances we can separate and therefore we considered that these resonances represent Ericson fluctuations. A similar estimate of the level density in $^{207}$Pb results in very large numbers, of the order of a few hundred levels per MeV. From Fig. 3 it is clear that we do not see such a large number of resonances. We can state that in the case of $^{207}$Pb, which is a much heavier nucleus then those previously reported, all structures we see in the cross sections are Ericson fluctuations.

Figure 4 shows the integral $\gamma$ production cross section of the 803.1-keV transition from the inelastic threshold up to 18 MeV. Only few experimental data points were found in the literature and significant discrepancies with most of these data are observed. The difference with the measured values of Lind *et al.* [15] increases with the increase of the incident

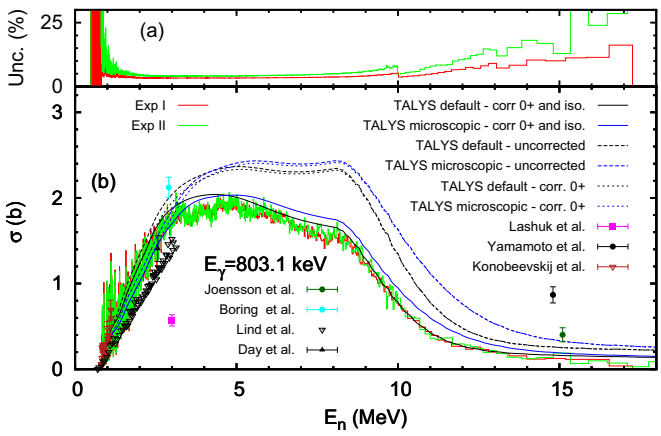


FIG. 4. (Color online) Integral $\gamma$ production cross section for the 803.1-keV transition in $^{206}$Pb. The upper panel represents the corresponding total uncertainty.

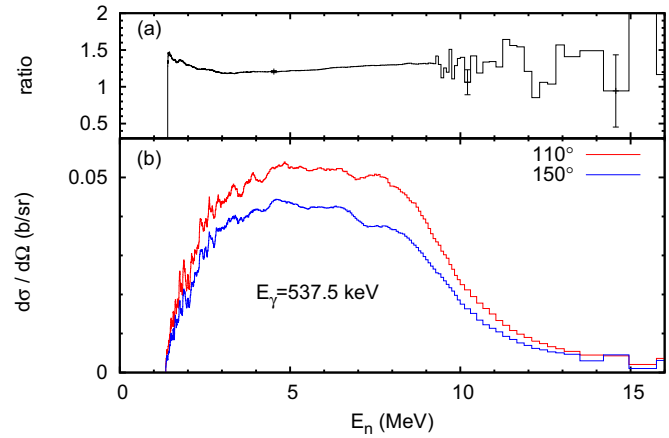


FIG. 5. (Color online) Differential $\gamma$ production cross section for the 537.5-keV transition in $^{206}$Pb at 110° and 150° together with the ratio between the differential cross section values. The data were smoothed with an averaging moving window filter for an easier comparison.

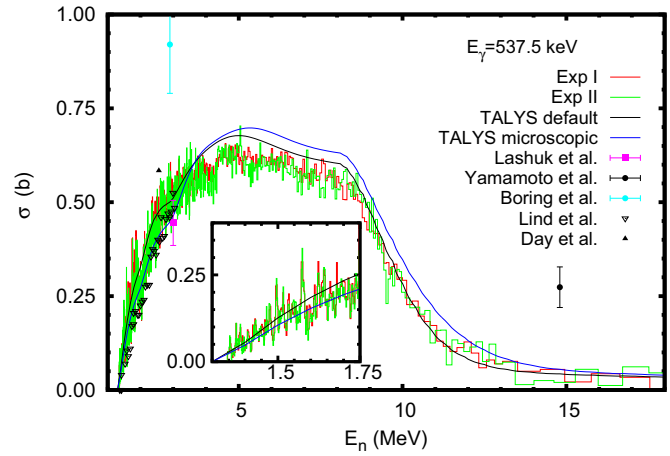


FIG. 6. (Color online) Integral $\gamma$ production cross section for the 537.5-keV transition in $^{206}$Pb from threshold to $E_n = 18$ MeV together with a zoom from the threshold up to 1.7 MeV, where the resonance structure is still visible.

neutron energy. The two data points of Lashuk *et al.* [66] and Yamamoto *et al.* [12] are very different compared with the present results: The first one is lower and the second one, at about 15 MeV, is higher. The point value of Boring *et al.* [14] is also slightly higher than our result at about 3 MeV while the point measured by Day *et al.* [16] in the same energy region is in good agreement with our data.

The total uncertainty of the integral $\gamma$ production cross section of the 803.1-keV $\gamma$ ray is shown in Fig. 4(a). Uncertainty of about 5% was obtained below 9 MeV with a continuous increase above this energy. The increase of the uncertainties at the limits of the measurement interval is from the low counting rate (small cross sections and lower neutron flux at high energies) while the drop at $E_n = 10$ MeV is from a different binning of the time-of-flight spectra starting at that value.

Several TALYS calculations are shown in Fig. 4, using both default (black lines) and the microscopically determined (blue lines) parameters. As discussed previously, the uncorrected calculations are shown using broken lines. The calculations corrected only for the branching ratio of the transition from the $0^+$ level are shown using dotted lines. The results of those calculations show that this correction does not play a significant role. The continuous lines display the fully corrected TALYS calculations, i.e., the correction for the isomeric level was applied. We point out that all other TALYS calculations displayed through the current article include the two corrections discussed above.

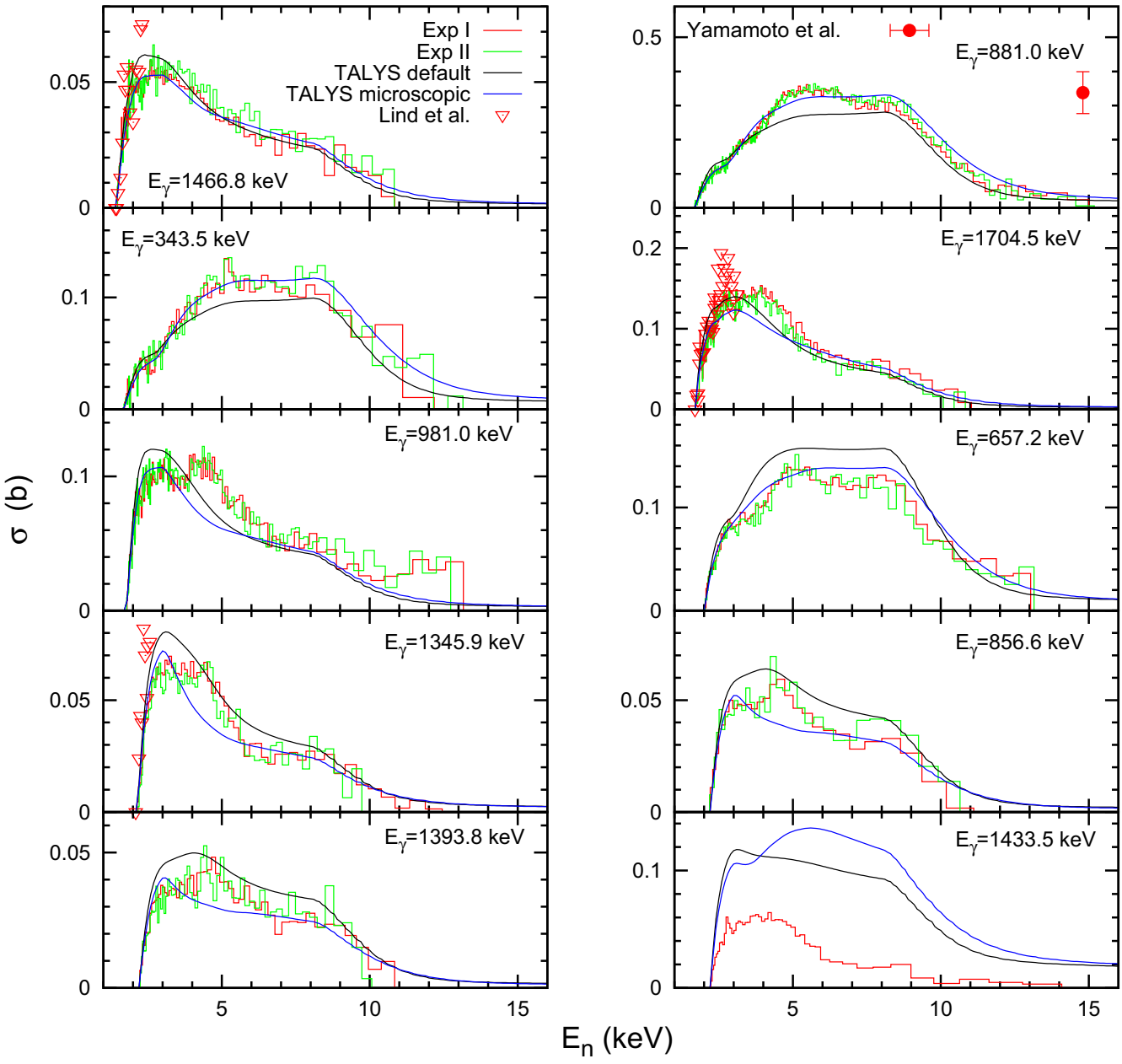


FIG. 7. (Color online) Integral $\gamma$ production cross section for the transitions from higher lying levels in $^{206}$Pb - 1/3.

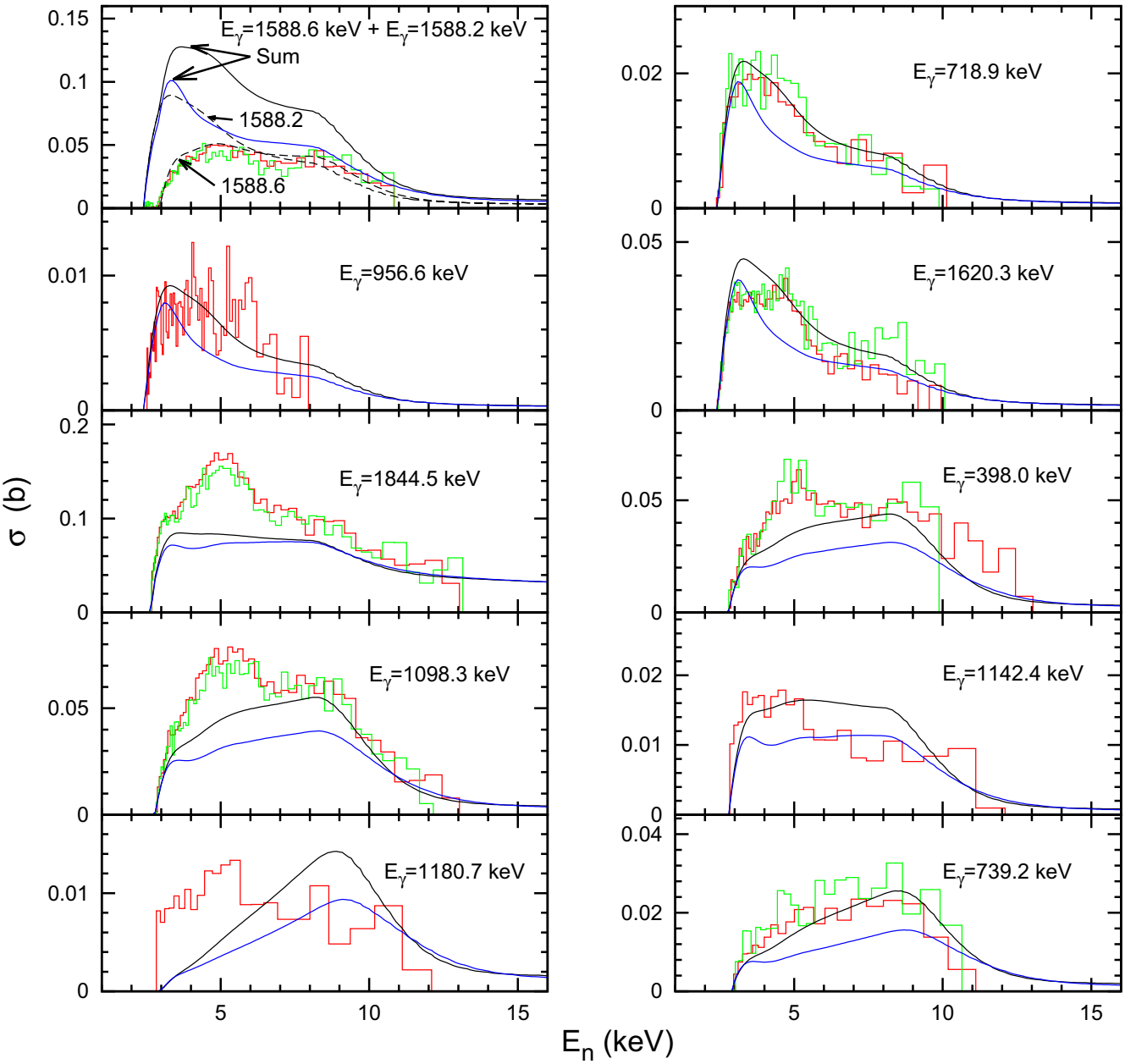


FIG. 8. (Color online) Integral $\gamma$ production cross section for the transitions from higher lying levels in $^{206}$Pb - 2/3.

#### 2. *The 537.5-keV transition*

Figures 5 and 6 show the differential and the integrated $\gamma$ production cross section of the 537.5-keV M1+E2 transition from the first $3^+$ level at 1340.5 keV to the $2^+$ level at 803.1 keV.

The two measurements from the present experiment overlap. The experimental data of Lashuk *et al.* [66], Day *et al.* [16], and Lind *et al.* [67] are relatively close to the present results whereas the measurements of (Boring *et al.* [14] and Yamamoto *et al.* [12]) are considerably higher. After the correction for the isomer, the TALYS calculation describes well the experimental data. A significant difference can still be observed between $E_n = 4$ and 8 MeV where the calculation is higher. Even if the 537.5-keV transition is the result of the decay of the third excited level, some resonance structures are still visible up to 1.7 MeV.

#### 3. *Transitions from higher lying levels*

Figures 7–9 show the integral $\gamma$ production cross section for transitions from excited levels above 1466.8 keV. Up to $E_x = 2236.5$ keV at least one $\gamma$ ray was observed decaying from each level. Above this energy some levels were not observed very probably because of their low cross section. The smaller $\gamma$ production cross section determined in this experiment has a maximum of about 10 mb (the 956.6-keV transition).

The $\gamma$ production cross section given for $E_\gamma = 1588$ keV is a sum of the $\gamma$ production cross sections of two transitions of 1588.2 and 1588.6 keV that decay from the levels at

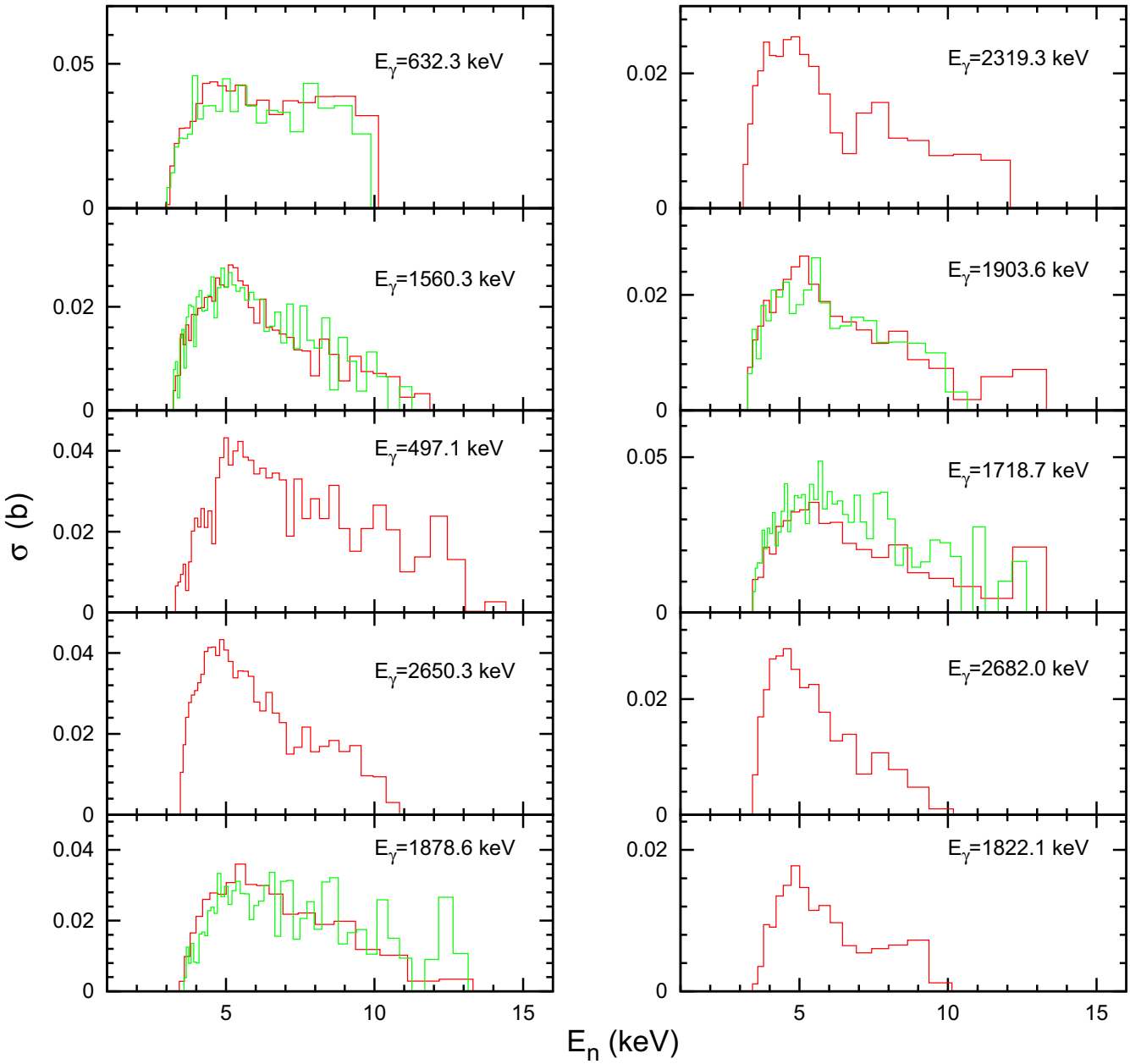


FIG. 9. (Color online) Integral $\gamma$ production cross section for the transitions from higher lying levels in $^{206}$Pb - 3/3.

2391.3 keV and at 2929.1 keV, respectively. The two $\gamma$ rays could not be distinguished with the present experimental setup. However, from the threshold observed in the $\gamma$ production cross section and from the comparison with TALYS (Fig. 8) it seems that the contribution from the $\gamma$ decaying from the 2391.3-keV level is negligible.

The most intense $\gamma$ ray from the level at 1466.8 keV ($E_\gamma = 663.8$ keV) was not measured in the present experiment because of a background peak at about the same energy.

Only the measurements of Yamamoto *et al.* [12] for the 881.0-keV transition and Lind *et al.* [67] for the 1466.8- and 1704.5-keV $\gamma$ rays were found in the literature (see Fig. 7). The Yamamoto *et al.* value for the production cross section of the 881.0-keV $\gamma$ ray is much higher than the present results. The data of Lind *et al.* for the 1466.8- and the 1704.5-keV transitions agree well with the present measurement up to about 2.5 MeV. Above this energy, the Lind *et al.* data are higher.

All TALYS calculations were corrected for the decay from the isomer. The calculations using the microscopic input parameters describe better the transitions at 657.2, 1345.9, 856.6, and 1393.8 keV while the default parameters describe better the 718.9- and 956.6-keV transitions. The code strongly overestimates the 1433.5-keV transition. One can conclude that no clear systematic difference was observed between the calculation and the experimental data.

However, a general overview of the $\gamma$ production cross sections and their comparison with the TALYS calculation reveals additional interesting information: In several cases

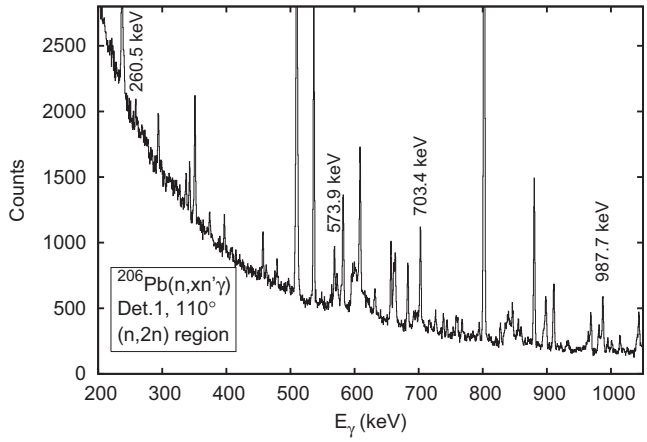


FIG. 10. $\gamma$ spectrum with the $^{\text{radiogenic}}$Pb sample integrated over neutron energies above 8.12 MeV up to about 25 MeV. The 260.5-, 573.9-, 703.4- and 987.7-keV peaks from the $^{206}$Pb$(n, 2n)^{205}$Pb reaction are visible.

the calculations are able to reproduce correctly the steplike features appearing in the shape of the excitation functions. This is the case for the steps observed at $E_n \approx 1.8$ MeV in the cross sections of the 881.0- and 343.5-keV transitions decaying from the 1684.0-keV level. Such features of the $\gamma$ production cross sections are probably caused by the excitation through the inelastic process of a level that further decays feeding the transition of interest: For $E_n \geqslant 1.8$ MeV the two transitions mentioned above start to be fed also through the decay of the 2782.8- and 2826.3-keV levels, both strongly connected with the 1684.0-keV level. Nevertheless, similar features in the shape of other $\gamma$ production cross sections are not correctly reproduced by TALYS. Clear examples are the 1704.5-, 981.0-, 1345.9-, and 856.6-keV transitions which display steplike features around $E_n = 3$–4 MeV. We interpret this disagreement as a sign of inconsistencies (possibly incorrect branching ratios or missing levels) in the level scheme of $^{206}$Pb used by TALYS. Because of the remarkable lack of selectivity of the $(n,n')$ reaction, the careful analysis of the excitation functions can therefore point out issues of the existing nuclear structure databases. Such a detailed analysis is, however, beyond the scope of the present article.

TABLE III. Branching ratios for levels in the $^{206}$Pb nucleus and the corresponding absolute uncertainties. The present results are compared with the values from the evaluated level scheme [37].

| $E_L$(keV) | $E_\gamma$ | Branching ratio | |
|---|---|---|---|
| | | Present result | Evaluated [37] |
| 1684.0 | 343.5 | 37.3(7) | 35.4(5) |
| | 881.0 | 100 | 100.0(1) |
| 2196.7 | 856.6 | 100 | 100 |
| | 1393.8 | 82.7(13) | 78(5) |
| 2423.4 | 718.92 | 63.5(21) | 48.5(20) |
| | 956.6 | 24.6(18) | 20.6(16) |
| | 1620.3 | 100 | 100(4) |
| 2782.2 | 398.0 | 81.8(15) | 79.6(7) |
| | 1098.3 | 100 | 100(11) |
| 3244.2 | 1246.5 | 36.9(37) | 22.2(21) |
| | 1560.3 | 100 | 100(5) |
| | 1903.6 | 104.2(36) | 92(4) |

#### 4. Branching ratios

In five cases, at least two $\gamma$ rays from the decay of the same excited level in $^{206}$Pb were observed with enough statistics to construct the $\gamma$ production cross sections. For these levels it was possible to deduce the ratio between the $\gamma$-ray intensities (branching ratios). These ratios were calculated from the corresponding $\gamma$ production cross sections. The values presented in Table III were deduced during the first measurement of the present work and were checked during the second one.

The measured thresholds of these $\gamma$ rays agree with the calculated ones. As additional verification of the $\gamma$-ray identification, the present measured branching ratios are constant, within the uncertainties, as a function of the neutron energy. The present results agree reasonably with most of the evaluated values [37], significant differences being observed for the $\gamma$ rays of 718.9 and 1246.5 keV.

#### 5. $\gamma$ production cross sections from the (n, 2n) channel

The threshold of the $(n, 2n)$ reaction on $^{206}$Pb is at 8.13 MeV. The spectrum using the $^{\text{radiogenic}}$Pb sample integrated over neutron energies above the $(n, 2n)$ threshold is shown in Fig. 10. Although four transitions from $^{205}$Pb are visible in

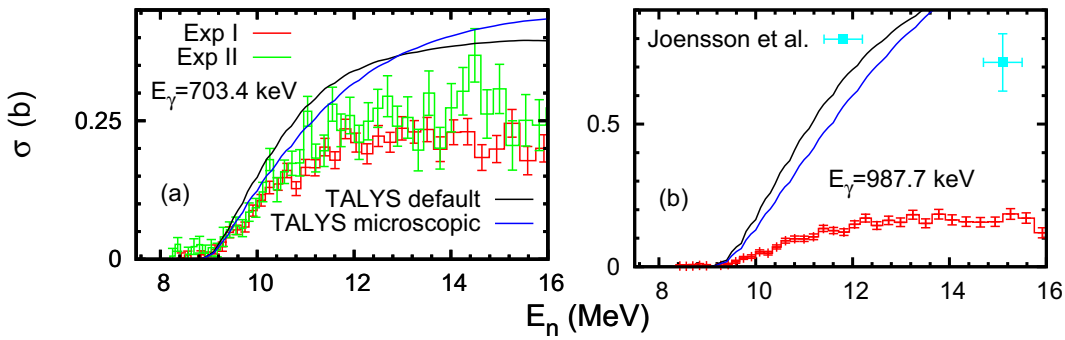


FIG. 11. (Color online) Integral production cross section for the $\gamma$ rays from the $^{206}$Pb$(n, 2n\gamma)^{205}$Pb reaction.

this integrated spectrum, we could build the production cross sections only for the 703.4- and 987.7-keV $\gamma$ rays, shown in Fig. 11. The observed experimental threshold of the $(n, 2n)$ transitions is the same as the theoretical value. The TALYS calculation overestimates the $\gamma$ production cross section of both transitions, which could be related to the existence of an isomer in $^{205}$Pb at 1013.9 keV: We note that in this case the TALYS calculations were not corrected for the existence of this isomer.

### B. Total inelastic and level cross sections

The total inelastic and level cross sections were constructed as described in Ref. [59] using the integral $\gamma$ production cross sections and the evaluated level scheme of $^{206}$Pb [37].

#### *1. Total neutron inelastic cross section*

For the construction of the total inelastic cross section we used the $\gamma$ transitions with $E_\gamma = 803.1$, 1466.8, 981.0, 1704.5, and 3194.6 keV (see Table II). The constructed total inelastic cross section does not include the contribution from the isomeric level at 2200.2 keV and from the $0^+$ level at 1166.4 keV. According to the level scheme of $^{206}$Pb, the first level that decays directly to the ground state and was not observed in the present experiment is at 3744.3 keV. This means that up to this energy the total inelastic cross section presented here is precise except for the contribution of the isomeric and of the $0^+$ levels. Above $E_n = 3.762$ MeV (which is the energy needed by a neutron to excite the 3744.3-keV level) the present curve is a low limit to the total inelastic cross section. However, this limit is very close to the precise value for $^{206}$Pb because in the present case most of the inelastic strength is collected through the first $\gamma$ transition, which is by far the most intense from the spectrum.

The total inelastic cross section obtained in Exp I is shown in Fig. 12 together with the corresponding total uncertainty. The total relative uncertainty is around 5% at $E_n \approx 2$ MeV and increases slowly at higher energies. The large values of the relative total uncertainty at the limits of the energy interval are from the poor statistics and correspond to very low values of the cross section.

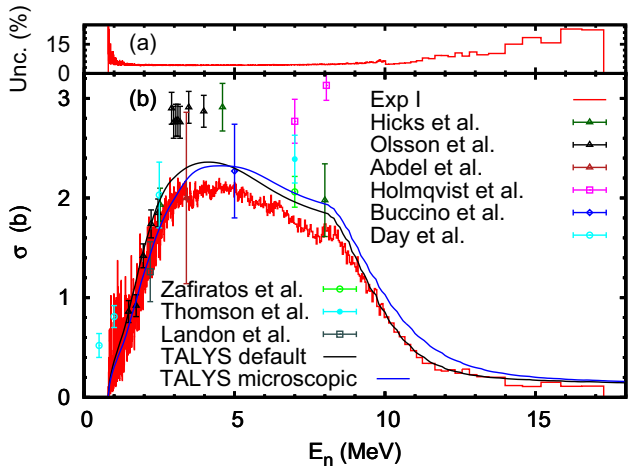


FIG. 12. (Color online) Total neutron inelastic cross section of $^{206}$Pb on full energy range up to 18 MeV. The upper panel represents the corresponding total uncertainty.

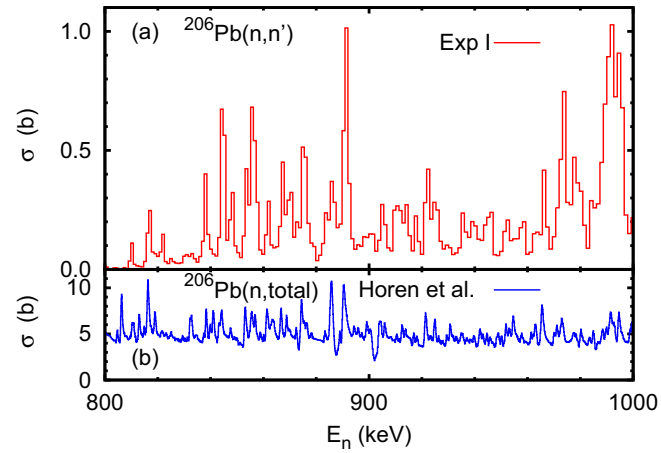


FIG. 13. (Color online) Full resolution total inelastic cross section compared with the neutron total cross section measured at the Oak Ridge Electron Linear Accelerator [68] with a transmission setup.

Several experimental points for the total inelastic cross sections found in the literature (Refs. [7,8,10,16,29,31,35]) are also displayed in Fig. 12. Our experimental data, with an uncertainty of the order of 5%, are much more precise than any previous measurement. We agree with the results of Landon *et al.* [8] and with Abdel *et al.* [67] in the low energy region, while the results of Holmqvist *et al.* [31], Thomson *et al.* [7], and Zafiratos *et al.* [35] at $E_n = 7$ MeV are higher than our data (however, as already stated, at this neutron energy one should regard our result as a lower limit of the total inelastic cross section). Although a good overlap with the data of Olson *et al.* [29] exists at low neutron energies, our results start to diverge at energies around 3–4 MeV.

The TALYS calculation with default parameters describes well the present results after the correction for the isomer and for the E0 transition, especially at very high neutron energy. It seems that the microscopic calculation follows better the

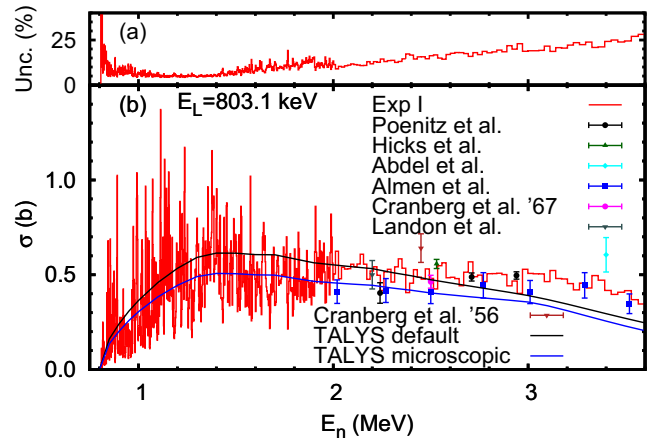


FIG. 14. (Color online) The cross section of the 803.1-keV level in $^{206}$Pb together with the corresponding total uncertainty.

shape of the cross section at low energies but fails above $E_n = 3$–4 MeV.

Figure 13 compares the inelastic cross section below 1 MeV with the total neutron cross section measured at the Oak Ridge Electron Linear Accelerator in a transmission experiment [68]. Despite the poorer neutron energy resolution of the present experiment, many of the resonances from the total cross section are seen also in the total inelastic cross section. Differences in the relative intensity between different resonances in the inelastic and in the total cross section exist. As an example, the two resonances at about 890 keV have almost the same intensity in the total cross section while in the inelastic cross section the resonance at 892 keV has higher intensity than the resonance at 886 keV. Also, we note that the absolute values of the inelastic cross section are a factor of ≈25 smaller than those of the total cross section (which includes the contributions from the capture and the elastic scattering).

### 2. *The 803.1-keV level*

The cross section of the first excited level is shown in Fig. 14. The first level not observed here that decays to the 803.1-keV level is at 2391.3 keV. Therefore, the cross section given here for the 803.1-keV level is precise up to 2.4 MeV.

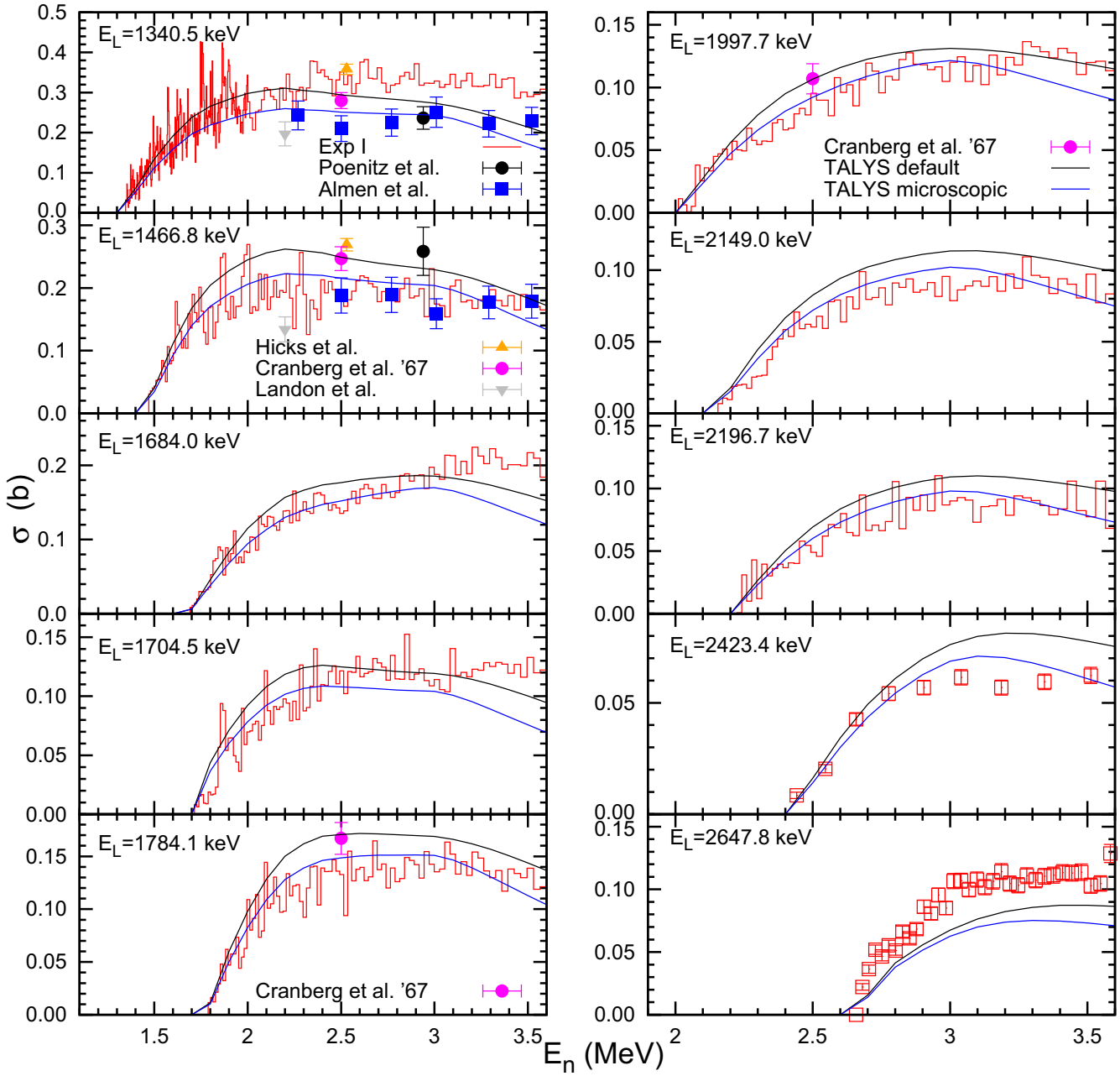


FIG. 15. (Color online) Cross section of excited levels above 1.3 MeV in $^{206}$Pb compared to previous experimental results and to TALYS calculations using default and microscopic parameters.

Above this energy, the curve from Fig. 14 is an upper limit for the 803.1-keV level cross section. The corresponding relative uncertainties are shown in Fig. 14(a).

The existing experimental data for this level cross section are mostly in good agreement with our result [4,6,8,9]. The data of Almen *et al.* [67] are lower, but just at the limit of one standard deviation of the two experiments while those of Cranberg *et al.* [6] and Abdel *et al.* [67] seem slightly too high.

The TALYS calculation describes well the cross section of the 803.1-keV level up to about 2.5 MeV. Above this energy, the calculation gives lower values. Part of this difference may come from the fact that the feeding from levels that were not observed above 2.4 MeV was neglected.

#### 3. *Levels with higher excitation energy*

Figure 15 shows cross sections of the levels with excitation energy between 1340.5 and 2647.8 keV. These cross sections were given only up to $E_n = 3.5$ MeV because 3606.2 keV is the highest excited level observed in this experiment.

Above 2.3-MeV excitation energy some excited levels were not observed. Therefore, above $E_n = 2.3$ MeV the level cross sections presented here should be considered as upper limits of the exact values. The difference reflects the intensity of the excited levels not observed in this experiment.

Previous experimental results were found for several levels. The data of Almen *et al.* [67] for the 1340.5-keV level are slightly too low but those for the 1466.8-keV level overlap perfectly with ours. At $E_n = 2.5$ MeV Cranberg *et al.* [6] display results that agree also with ours.

TALYS calculations using default and microscopic input parameters are plotted together with the present results (Fig. 15). Below 2.3-MeV neutron energy, the agreement between the calculation and the present measurement is good for the majority of the levels presented here. Above 2.5 MeV, the calculation gives lower values than the present measurement for the levels at 1340.5, 1684.0, and 2647.8 keV. These differences confirm our interpretation of the present results as lower limits of the cross sections above 2.3 MeV. Finally, we note that the agreement with TALYS seems to improve in several cases when the microscopic parameters are used.

## V. CONCLUSIONS

The neutron inelastic and the $(n, 2n\gamma)$ cross sections on $^{206}$Pb were measured with an unprecedented neutron energy resolution from threshold up to $E_n = 18$ MeV. Two measurements were performed using different samples and different acquisition systems and the very good agreement between the two measurements increased the confidence in the results. The good resolution of the HPGe detectors allowed the identification of 34 $\gamma$ rays from the inelastic channel and two $\gamma$ rays from the $(n, 2n\gamma)$ channel. Angle-integrated $\gamma$ production cross sections were determined for all these transitions. The total uncertainty for the most intense transition was about 5% below 9 MeV. The maximum observed excitation energy was 3.6 MeV for the inelastic scattering. A neutron energy resolution of 1.1 keV at 1 MeV allowed the observation of resonant structures for the first time in the inelastic scattering on $^{206}$Pb up to $E_n \approx 1.7$ MeV. However, a comparison of the number of resonancelike structures observed with the estimated level density in $^{207}$Pb around the excitation energy $S_n + E_n$ suggests that these structures represent only Ericson fluctuations.

In several cases, we were able to infer, based on our $\gamma$ production cross sections, new branching ratios. These are mostly in good agreement with the existing evaluated values.

The total inelastic and the level cross section were constructed relying on the present evaluated level scheme of $^{206}$Pb and using the angle-integrated $\gamma$ production cross sections. The level cross sections are precise up to 2.3 MeV while above this threshold they represent upper limits. The total inelastic cross section determined here does not include the contribution from the isomer level at 2200.2 keV and from the $0^+$ level at 1166.4 keV. Excluding these, our result for the total inelastic cross section is accurate up to 3.2 MeV; above this energy it is only a lower limit to the total inelastic cross section.

The present results were compared with existing experimental data found in the literature and with calculations performed with Version 1.6 of the TALYS code. The theoretical calculations were performed using default parameters but also a set of microscopically determined parameters and were corrected for the existence of a $0^+$ and an isomeric level in the low excitation energy level scheme of $^{206}$Pb. There is a good overall agreement between the present data and the calculations, mainly because of the optical model parameters which are known well in the mass region of the lead isotopes. Moreover, no clear improvement was obtained by using microscopically determined parameters. Finally, we note that the comparison between the shape of several experimental $\gamma$ production cross sections and the corresponding TALYS calculations seems to indicate possible deficiencies in the level scheme of $^{206}$Pb.

## ACKNOWLEDGMENTS

The authors thank the team of GELINA operators for the quality of the neutron beam, A. Moens and C. Quétel for preparation and characterization of the sample, and R. Wynants for technical support. A.N., L.C.M., and C.B. are grateful to IRMM for financial support. This work was partially supported by the European Commission within the Sixth Framework Programme through the EUROTRANS (EURATOM Contract No. 516520) and EFNUDAT (EURATOM Contract No. 036434) projects and within the Seventh Framework Programme through the CHANDA project (EURATOM Contract No. FP7-605203).

[1] G. Aliberti, G. Palmiotti, M. Salvatores, and C. G. Stenberg, Nucl. Sci. Eng. **146**, 13 (2004).

[2] G. Aliberti *et al.*, Ann. Nucl. Energy **33**, 700 (2006).

[3] M. Salvatores (coordinator) and R. Jacqmin (monitor), NEA/WPEC-26 report, Vol. 26 (NEA/WPEC, Issy-les-Moulineaux, 2008).

[4] S. F. Hicks, J. M. Hanly, S. E. Hicks, G. R. Shen, and M. T. McEllistrem, Phys. Rev. C **49**, 103 (1994).
[5] E. Almén-Ramström, Report AE-503 (Aktiebolaget Atomenergie, Studsvik, Nyköping, Sweden, 1975).
[6] L. Cranberg, T. A. Oliphant, J. Levin, and C. D. Zafiratos, Phys. Rev. **159**, 969 (1967).
[7] D. Thomson, Phys. Rev. **129**, 1649 (1963).
[8] H. H. Landon, A. J. Elwyn, G. N. Glasoe, and S. Oleksa, Phys. Rev. **112**, 1192 (1958).
[9] E. Poenitz, R. Nolte, D. Schmidt, and G. Chen, J. Korean Phys. Soc. **59**, 1876 (2011).
[10] S. G. Buccino, C. E. Hollandsworth, H. W. Lewis, and P. R. Bevington, Nucl. Phys. **60**, 17 (1964).
[11] J. K. Dickens, Phys. Rev. C **28**, 916 (1983).
[12] T. Yamamoto, Y. Hino, S. Itagaki, and K. Sugiyama, J. Nucl. Sci. Technol. **15**, 797 (1978).
[13] B. Jönsson, K. Nyberg, and I. Bergqvist, Arkiv för Fysik **39**, 295 (1969).
[14] J. W. Boring and M. T. McEllistrem, Phys. Rev. **124**, 1531 (1961).
[15] D. A. Lind and R. B. Day, Ann. Phys. **12**, 485 (1961).
[16] R. B. Day, Phys. Rev. **102**, 767 (1956).
[17] R. M. Kiehn and C. Goodman, Phys. Rev. **95**, 989 (1954).
[18] G. N. Salaita and P. K. Eapen, J. Inorg. Nucl. Chem. **35**, 2139 (1973).
[19] K. C. Garg and C. S. Khurana, Indian J. Pure Appl. Phys. **17**, 525 (1979).
[20] J. Fréhaut, A. Bertin, R. Bois, and J. Jary, in *Symposium on Neutron Cross Sections from 10–50 MeV* (BNL-NNDC, Upton, 1980).
[21] D. J. Horen, J. A. Harvey, and N. W. Hill, Phys. Rev. C **20**, 478 (1979).
[22] B. A. Benetskij, A. B. Kljachko, V. V. Nefjodov, I. M. Frank, and I. V. Shtranikh, Yad. Fyz. **17**, 21 (1973).
[23] D. G. Foster Jr. and D. W. Glasgow, Phys. Rev. C **3**, 576 (1971).
[24] A. D. Carlson and H. H. Barschall, Phys. Rev. **158**, 1142 (1967).
[25] J. V. Dukarevich, A. N. Djumin, and D. M. Kaminker, Nucl. Phys. A **92**, 433 (1967).
[26] G. M. Haas and P. L. Okhuysen, Phys. Rev. **132**, 1211 (1963).
[27] J. H. Coon, E. R. Graves, and H. H. Barschall, Phys. Rev. **88**, 562 (1952).
[28] D. W. Miller, R. K. Adair, C. K. Bockelman, and S. E. Darden, Phys. Rev. **88**, 83 (1952).
[29] N. Olsson, B. Holmqvist, and E. Ramström, Nucl. Phys. A **385**, 285 (1982).
[30] J. C. Ferrer, J. D. Carlson, and J. Rapaport, Nucl. Phys. A **275**, 325 (1977).
[31] B. Holmqvist and T. Wiedling, Report AE-482 (Aktiebolaget Atomenergie, Studsvik, Nyköping, Sweden, 1973).
[32] G. E. Belovitskij, L. N. Kolesnikova, and I. M. Frank, Yad. Fyz. **15**, 662 (1972).
[33] B. Holmqvist and T. Wiedling, Report AE-430 (Aktiebolaget Atomenergie, Studsvik, Nyköping, Sweden, 1971).
[34] S. G. Buccino, C. E. Hollandsworth, and P. R. Bevington, Z. Phys. **196**, 103 (1966).
[35] C. D. Zafiratos, T. A. Oliphant, J. S. Levin, and L. Cranberg, Phys. Rev. Lett. **14**, 913 (1965).
[36] A. D. Carlson *et al.*, Nucl. Data Sheets **110**, 3215 (2009).
[37] F. G. Kondev, Nucl. Data Sheets **109**, 1527 (2008).
[38] A. J. Koning and J. P. Delaroche, Nucl. Phys. A **713**, 231 (2003).
[39] A. J. Koning and M. C. Duijvestijn, Nucl. Phys. A **744**, 15 (2004).
[40] A. J. Koning, S. Hilaire, and S. Goriely, Nucl. Phys. A **810**, 13 (2008).
[41] R. Capote *et al.*, Nucl. Data Sheets **110**, 3107 (2009).
[42] E. Bauge, J. P. Delaroche, and M. Girod, Phys. Rev. C **58**, 1118 (1998).
[43] E. Bauge, J. P. Delaroche, and M. Girod, Phys. Rev. C **63**, 024607 (2001).
[44] S. Hilaire and S. Goriely, Nucl. Phys. A **779**, 63 (2006).
[45] S. Goriely, S. Hilaire, and A. J. Koning, Phys. Rev. C **78**, 064307 (2008).
[46] A. J. Koning and M. C. Duijvestijn, Nucl. Instrum. Meth. Phys. Res. B **248**, 197 (2006).
[47] A. J. Koning and D. Rochman, Nucl. Data Sheets **113**, 2841 (2012).
[48] L. C. Mihailescu, L. Oláh, C. Borcea, and A. J. M. Plompen, Nucl. Instrum. Meth. Phys. Res. A **531**, 375 (2004).
[49] L. Mihailescu, C. Borcea, A. Koning, and A. Plompen, Nucl. Phys. A **786**, 1 (2007).
[50] L. C. Mihailescu, C. Borcea, and A. Plompen, Nucl. Instrum. Meth. Phys. Res. A **578**, 298 (2007).
[51] D. Ene, C. Borcea, S. Kopecky, W. Mondelaers, A. Negret, and A. Plompen, Nucl. Instrum. Meth. Phys. Res. A **493**, 106 (2002).
[52] M. Flaska, A. Borella, D. Lathouwers, L. C. Mihailescu, W. Mondelaers, A. J. M. Plompen, H. van Dam, and T. H. J. J. van der Hagen, Nucl. Instrum. Meth. Phys. Res. A **531**, 392 (2004).
[53] D. Tronc, J. M. Salomé, and K. Böckhoff, Nucl. Instrum. Meth. Phys. Res. A **228**, 217 (1985).
[54] J. F. Briesmeister, Report LA-13709-M (Los Alamos National Laboratory, Los Alamos, 2000).
[55] D. Deleanu, C. Borcea, Ph. Dessagne, M. Kerveno, A. Negret, A. J. M. Plompen, and J. C. Thiry, Nucl. Instrum. Meth. Phys. Res. A **624**, 130 (2010).
[56] L. C. Mihailescu, Report EUR 22343 EN (European Communities, 2006).
[57] R. Nolte and D. J. Thomas, Metrologia **48**, S274 (2011).
[58] A. Plompen *et al.*, J. Korean Phys. Soc. **59**, 1581 (2011).
[59] C. Rouki, P. Archier, C. Borcea, C. De Saint Jean, J. C. Drohé, S. Kopecky, A. Moens, N. Nankov, A. Negret, G. Noguère, A. J. M. Plompen, and M. Stanoiu, Nucl. Instrum. Meth. Phys. Res. A **672**, 82 (2012).
[60] A. J. Koning, S. Hilaire, and M. C. Duijvestijn, in *Proceedings of the International Conference on Nuclear Data for Science and Technology - ND2004* (AIP Conference Proceedings, Melville, 2005), p. 1154.
[61] J. Raynal, Technical Report CEA-N-2772 (CEA, Saclay, 1994).
[62] E. Sheldon and V. C. Rogers, Comput. Phys. Commun. **6**, 99 (1973).
[63] A. Negret, C. Borcea, Ph. Dessagne, M. Kerveno, A. Olacel, A. J. M. Plompen, and M. Stanoiu, Phys. Rev. C **90**, 034602 (2014).
[64] A. Olacel, C. Borcea, Ph. Dessagne, M. Kerveno, A. Negret, and A. J. M. Plompen, Phys. Rev. C **90**, 034603 (2014).
[65] T. von Egidy and D. Bucurescu, Phys. Rev. C **72**, 044311 (2005).
[66] A. I. Lashuk and I. P. Sadokhin, Vop. At. Nauki i Tekhn., Ser. Yadernye Konstanty **1996**(2), 59 (1996).
[67] EXFOR/CSISRS, Nuclear reaction data [www.nndc.bnl.gov], [www.nea.fr/html/dbdata/x4/x4ret.html], or [www-nds.iaea.or.at/exfor].
[68] D. J. Horen, J. A. Harvey, and N. W. Hill, Phys. Rev. C **24**, 1961 (1981).